Heat transfer of the multicolor-laser-sources-irradiated nanoparticles in reference to thermal processes

Piotr Radomski[a], Federica Zaccagnini[b], Paweł Ziółkowski[a], Francesca Petronella[c], Luciano de Sio[b] and Dariusz Mikielewicz[a]

[a]Gdansk University of Technology, Faculty of Mechanical Engineering and Ship Technology, Energy Institute, Poland;
[b]Sapienza University of Rome, Department of Medico-surgical Sciences and Biotechnologies, Italy;
[c]Insitute of Crystallography of National Research Council, Department Chemical Sciences and Material Technologies, Italy

Abstract:

Unlike the standard materials, metallic nanoparticles offer enhancing the heat convertion rate which implies the maximum and average temperature boost significantly in the considered system. The work's purpose is to examine heat transfer in the metallic nanoparticles which have been deposited on a glassy substrate, enabling the nanostructures thermoablation. Furthermore, the functionalized substrate is irradiated with multicolor-laser-sources, with a future perspective to develop a solar model. This is particularly crucial at improving efficiency in solar-collectors-based renewable energy sources. On the other hand, the theoretical investigations which have been previously verified for a single laser source aim to demonstrate the unsteady temperature and entropy increase in selected geometry cross-sections. The produced heat and the appropriate boundary conditions are calculated based on the advanced optics (Mie-Lorentz and Rayleigh-Drude theories) using an analytical approach. On the other hand, the temperature field and entropy production for the case study is being achieved via CFD simulations. The obtained results will be subsequently being applied in order to optimize the appropriate nanoparticle size and shape in operational work conditions.

Keywords:

heat transfer, light ablation, energy convertion, nanostructures

1. Introduction

The world sources of energy were grounded on fossil fuels above one hundred years ago due to their efficiency and common availability. It has been discovered, however, that their exploitation and extensive utilization is contributing to have the greenhouse effect accelerated. Therefore, the diligent search of new alternate energy sources and their diversification has been a burning issue nowadays. Nonetheless, the majority of the renewable sources of energy do not provide the instant and powerful temperature increase at the same time, which may last either long hours or explode the costs of usage. Regrettably, many of the available techniques are based on the heat flux supply to the fluid-solid boundary, which implies a slow temperature increase in the whole system [1].

On the other hand, since the COVID-19 pandemic situation began, the peoples have realized the necessity of hand and room disinfections. Unlike the powerful chemical compounds, the overheating of viruses by reaching an appropriate temperature may reduce number of germs in a selected volume to virtually zero. In a similar way, tumors and cancers could be damaged completely, however there is the same problem with penetration in order not to kill healthy cells at the same time and in order to provide the noninvasiveness [2–3].

In this moment, metallic nanoparticles emerge as a new strategy by using their own radiative properties. Their advantage is that they may freely travel through a microscale pipe, which increases temperature much faster than it is performed with a standard metal sheet. The future perspective is to apply them as an agent for solar collectors, steam production or germs inactivation. Although there are several papers which propose the nanofluidic flows in the context of mass and heat transfer [4 – 5], heat generation and nanoparticles' shape optimization are an abstruse issue and require to compute sophisticated formulas and equations that would be calculated numerically.

Therefore, this work introduces and offers step by step some theoretical methods which are joined following the available models, which is Cattaneo-Vernotte equation for nanoparticles, Rayleigh-Drude approximation, Royer-Yamaguchi approach for a surface effect and the electromagnetic energy convertion into heat, which has been developing in authors' papers. Likewise, the proposed theory is capable of being shifted for bulbs

https://doi.org/10.52202/069564-0033

and solar models. Moreover, the obtained results for the selected theory are revealed for the specially-prepared system which was thermoablated using three lasers and which enables to study both convection moves and microscale heat transfer effects.

2. Theoretical models

Heat transfer of light-ablated metallic nanoparticles is calculated in different methods, depending on the considered model. Nevertheless, most of them require using the hyperbolic energy equation, which is known as Cattaneo-Vernotte equation [7 – 8], and frequently is dedicated for pulsed light sources where temperature inside nanoparticles cannot be written as constant the whole time. For AuNRs, this equation is presented as follows:

$$\mathrm{r}\cdot\frac{\partial^2}{\partial t^2}(\rho\cdot e)+\frac{\partial}{\partial t}(\rho\cdot e)=\mathrm{div}\big(k_{\mathrm{eff}}\cdot\mathrm{grad}(T)\big)+S_e^{\mathrm{np}} \tag{1}$$

$$\mathrm{r}=3\cdot\frac{k_{\mathrm{eff}}}{\rho\cdot c_p}\cdot\frac{1}{{v_{\mathrm{sound}}}^2} \tag{2}$$

On the other hand, for the continuous light sources, like CW-lasers, the delivered heat is sufficiently low so as to have the hyperbolic energy equation reduced into the standard parabolic one. In this work, including gravity forces and Boussinesq approach, the utilized continuity, momentum and energy, turbulence and dissipation equations are written by [5]:

$$\frac{\partial}{\partial t}\begin{Bmatrix}\rho\\ \rho\vec{v}\\ \rho e\\ \rho\mathbb{k}\\ \rho\epsilon\end{Bmatrix}+\mathrm{div}\begin{Bmatrix}\rho\vec{v}\\ \rho\vec{v}\otimes\vec{v}\\ \rho e\vec{v}\\ \rho\mathbb{k}\vec{v}\\ \rho\epsilon\vec{v}\end{Bmatrix}=\mathrm{div}\begin{Bmatrix}0\\ \overrightarrow{\tau}-p\overrightarrow{I}\\ \left(\overrightarrow{\tau}-p\overrightarrow{I}\right)\cdot\vec{v}+(k_{\mathrm{eff}}+k_{\mathrm{t}})\cdot\mathrm{grad}(T)\\ \left(\mu+\frac{\mu_{\mathrm{t}}}{\mathrm{Pr}_{\mathbb{k}}}\right)\cdot\mathbb{k}\\ \left(\mu+\frac{\mu_{\mathrm{t}}}{\mathrm{Pr}_{\epsilon}}\right)\cdot\epsilon\end{Bmatrix}+\begin{Bmatrix}0\\ (\rho-\rho_o)\cdot\vec{g}\\ S_e^{\mathrm{f}}+S_e^{\mathrm{np}}\\ G_{\mathbb{k}}-\rho\epsilon+G_{\mathrm{Б}}\\ C_{1\epsilon}\cdot\frac{\epsilon}{\mathbb{k}}\cdot\left(G_{\mathbb{k}}+C_{3\epsilon}\cdot G_{\beta}\right)-C_{1\epsilon}\cdot\rho\cdot\frac{\epsilon^2}{\mathbb{k}}\end{Bmatrix} \tag{3}$$

where:

$$\overrightarrow{\tau}=\mathrm{grad}\left(\overrightarrow{X^{\dagger}}\right)-\frac{2}{3}\mu I_{\overrightarrow{d}}\overrightarrow{I}+2\mu\overrightarrow{d}-\frac{2}{3}(\rho\mathbb{k}+\mu_{\mathrm{t}}\cdot I_{\overrightarrow{d}})\cdot\overrightarrow{I}+2\mu_{\mathrm{t}}\cdot\overrightarrow{d} \tag{4}$$

$$G_{\mathbb{k}}=2\mu_{\mathrm{t}}\cdot\overrightarrow{d}\cdot\overrightarrow{d^{\dagger}} \tag{5}$$

$$G_{\mathrm{Б}}=\mathrm{Б}\cdot\frac{\mu_{\mathrm{t}}}{\mathrm{Pr}}\cdot\vec{g}\cdot\mathrm{grad}(T) \tag{6}$$

The most relevant factors, however, estimate this part of energy which is directly converted into heat from the incident light. Likewise, the formulas may be presented for fluids (and solids as well) and particles, respectively as follows:

$$S_e^{\mathrm{f}}=A_{abs_M}\cdot I_{abs_M}=A_{abs_M}\cdot I_o(\vec{r})\cdot(1-R_M)\cdot\left(1-\exp\left(-A_{abs_M}\cdot\delta\right)\right) \tag{7}$$

$$S_e^{\mathrm{np}}=\sum_{i=1}^{N}A_{abs_i}\cdot I_{abs_i}=\sum_{i}^{N}w_i\cdot\left(\xi\cdot C_{abs_i}\cdot I_o(\vec{r})\cdot(1-R_i)\cdot\left(1-\exp\left(-A_{abs_i}\cdot l_{ph}\right)\right)\right) \tag{8}$$

The difference is visible as well in the absorption coefficient whose value is calculated via different ways. For continuous media, like homogeneous fluids or solids, the formula may be described by:

$$A_{abs_M}=\frac{4\pi\cdot\mathbb{Im}\left(n_M(\lambda)\right)}{\lambda} \tag{9}$$

For particles, however, the formula implies counting particle by particle, which obviously cannot be performed. This is the reason why N refers to the number of the grouped particles which possess the same or similar dimensions. The commonly utilized theory, which solves the problem, is based on Rayleigh-Drude approximation whose advantage is the simplicity in adjusting both size, shape and distance effects [9 – 10]. The general formula are followed by [11 – 12]:

$$A_{abs_i}=\xi\cdot\left(\left(C_{ext_i}\right)-\left(C_{sca_i}\right)\right)=\xi\cdot\left(\left(4\pi\cdot\left(\frac{2\pi}{\lambda}\right)\cdot\mathbb{Im}(\alpha_i)\right)-\left(\frac{8\pi}{3}\cdot\left(\frac{2\pi}{\lambda}\right)^4\cdot|\alpha_i|^2\right)\right) \tag{10}$$

Nevertheless, the situation which significantly distinguishes the converted rate is how far from the surface nanoparticles are located. For microsize pipes this effect is relevant only near walls, and here only nanofluidic theories are utilized based on the heat transfer coefficient between fluid and particles [4 – 5]. Amongst many theories where the topic has been investigated, Smoluchowski theory, which is presented in [13 – 14], provides satisfactory solutions.

https://doi.org/10.52202/069564-0033

On the other hand, when nanoparticles are deposited on a surface, the interaction should be included with the surface effect which generally increases the optical cross sections, especially for elongated shapes, like nanodisks or nanorods. Here, Royer-Yamaguchi approach [15 – 16] appears to be a perfect solution due to the fact it includes both the surface and distance effect. In this work, the adjusted polarizabilities for rods are presented in the Appendix A. Nevertheless, it should be mentioned that this method is immature for prolate structure, and provides the validity only for the symmetrical alignment of nanoparticles to each other. The other configurations, although they correspond much more to reality, are not supported with the abovementioned formulas, and this aspect would be under further investigations.

Furthermore, total entropy generation, $\mathbb{S}$, is investigated using formula [21,33 – 35] for Boussinesq and turbulent approach:

$$\mathbb{S} = \left(\frac{k_{\text{eff}} + k_{\text{t}}}{T^2}\right) \cdot \left(\text{grad}(T)\right)^2 + \left(\frac{\mu}{T}\right) \cdot \left(-\frac{2}{3} I_{\vec{d}} \cdot \vec{I} + 2\vec{d}\right) + \left(\frac{1}{T}\right) \cdot \left(-\frac{2}{3}(\rho \mathbb{k} + \mu_{\text{t}} I_{\vec{d}})\vec{I} + 2\mu_{\text{t}}\vec{d}\right) \tag{11}$$

This parameter determines the irreversibility rate of each process, and may reveal which irreversible processes, friction in movement or heat transfer with conduction and forced or natural convection is dominant at each stadium of the simulations.

3. Numerical proceedings

3.1. Considered system

In order to reduce the number of examined systems and to investigate the heat and mass transfer particularly at the same time, it has been decided to create the model which is both simple to prepare, to simulate and to be proceeded in the target application. Fig. 1. outlines the system's scheme from two sides. Gravitational forces works along the x direction in this model.

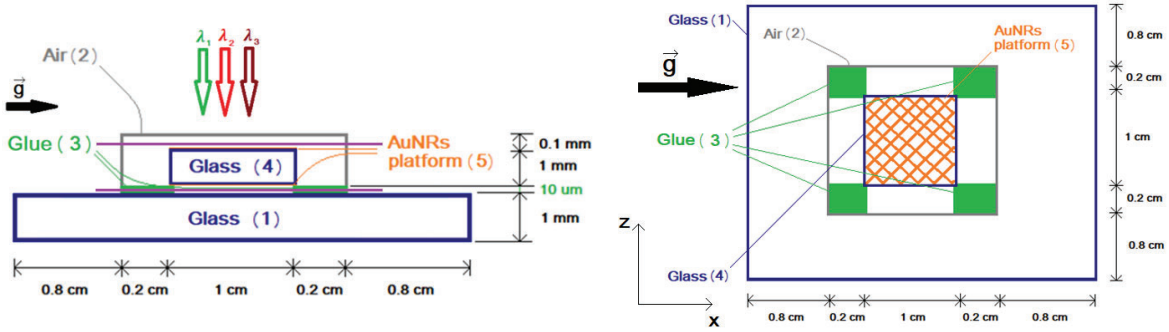

Figure. 1. Scheme of the created geometry and domains with boundary conditions applied in the simulations (scale has not been saved). Violet lines highlight the considered planes in section "Results".

3.2. Boundary conditions

In order to compute the results numerically, the considered system has been discretized into three grids. The calculations have been performed via *Ansys.Fluent* software (version 22.1) on the *Tryton* supercomputer of the TASK resources consisted of 72 cores (Intel®Xeon®Processor E5 v3 @ 2,3GHz) using the SIMPLE algorithm and the second-order scheme for the (2) – (9) equations. The control parameters have been established on 0.5 excepting pressure and density whose values equals 0.3. The space and time tests are based on Roacher's and Richardson's extrapolations [17] so as to verify and minimize the numerical error. The utilized mesh for results is visible in fig. 2.

Likewise, boundary conditions are specified assuming the system is kept in the adiabatic conditions, excepting the irradiated walls where mixed conditions are expected. Moreover, diffusive momentum flux, although they are coated on the glassy base, require using Marangoni's stress for gold nanoparticles due to the presence of the organic compound (CTAB):

$$\overrightarrow{X^{\dagger}} \rightarrow \frac{d\vec{\sigma}}{dT} \cdot \text{grad}(T) \tag{13}$$

where surface tension coefficient equals $\frac{d\vec{\sigma}}{dT} = -0.00005263\ \text{N} \cdot \text{m}^{-1} \cdot \text{K}^{-1}$ [21].

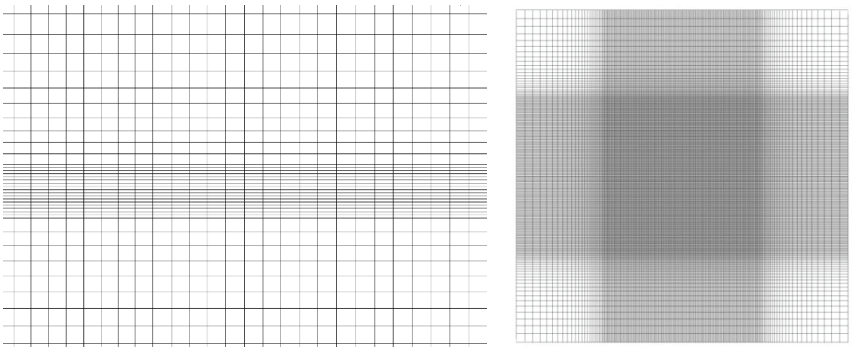

Figure. 2. Applied discretized grid in the simulations from two sides.

Furthermore, heat source, which are three lasers here with the incident wavelengths, $\lambda_{L=1} = 532\ \mathrm{nm}$, $\lambda_{L=2} = 640\ \mathrm{nm}$, $\lambda_{L=3} = 808\ \mathrm{nm}$, undergo the gaussian distribution in the space regime, accordingly:

$$S_e^{\mathrm{np}} = \sum_{L=1}^{3}\left(\sum_{i}^{N} w_i \cdot \left(\xi \cdot C_{abs_i}(\lambda_L) \cdot I_{oL} \cdot \exp\left(-2\left(\frac{\vec{r}}{R_{\phi L}}\right)^2\right) \cdot \left(1 - R_i(\lambda_L)\right) \cdot \left(1 - \exp\left(-A_{abs_i}(\lambda_L) \cdot l_{ph}\right)\right)\right)\right) \tag{14}$$

where each laser output power has been established on $80\ \mathrm{mW}$. These three lasers deliver the heat flux during 90 seconds (irradiation time). After this time, the system is being cooled.

Table 1. details all mentioned assumptions, whereas table 2. reveals material thermal properties from literature.

Table 1. Specified boundary conditions in the considered simulations

No.	Material	Type of boundary conditions	Details
(1)	Bottom borosilicate glass	Mixed	$T_o = 297.15\ \mathrm{K}\ (75.20^{\mathrm{o}}\mathrm{F})$ $h = 13.6\ \mathrm{W \cdot m^{-2} \cdot K^{-1}}$ $\delta = 0.001\ \mathrm{m}$ $S_e^{\mathrm{f}} \approx 0\ \mathrm{W \cdot m^{-3}}$ $R_{\phi L} = 0.0015\ \mathrm{m}$
(2)	Air	Outlet (Neumann)	$T_o = 297.15\ \mathrm{K}\ (75.20^{\mathrm{o}}\mathrm{F})$ $v_o = 0$ $S_e^{\mathrm{f}} \approx 0\ \mathrm{W \cdot m^{-3}}$
(3)	Glue	Neumann	$T_o = 297.15\ \mathrm{K}\ (75.20^{\mathrm{o}}\mathrm{F})$ $S_e^{\mathrm{f}} \approx 0\ \mathrm{W \cdot m^{-3}}$
(4)	Top borosilicate glass	Mixed	$T_o = 297.15\ \mathrm{K}\ (75.20^{\mathrm{o}}\mathrm{F})$ $h = 13.6\ \mathrm{W \cdot m^{-2} \cdot K^{-1}}$ $\delta = 0.001\ \mathrm{m}$ $S_{e_1}^{\mathrm{f}} = 0.0006956\ \mathrm{W \cdot m^{-3}}$ $S_{e_2}^{\mathrm{f}} = 0.0015740\ \mathrm{W \cdot m^{-3}}$ $S_{e_3}^{\mathrm{f}} = 0.0003483\ \mathrm{W \cdot m^{-3}}$ $R_{\phi L} = 0.0015\ \mathrm{m}$
(5)	Gold surface	Neumann	$T_o = 297.15\ \mathrm{K}\ (75.20^{\mathrm{o}}\mathrm{F})$ $l_{ph} = 26.0\ \mathrm{nm}$ $S_{e\ 1}^{\mathrm{np}} = 1.45745 \cdot 10^{11}\ \mathrm{W \cdot m^{-3}}$ $S_{e\ 2}^{\mathrm{np}} = 1.90629 \cdot 10^{9}\ \mathrm{W \cdot m^{-3}}$ $S_{e\ 3}^{\mathrm{np}} = 3.22348 \cdot 10^{11}\ \mathrm{W \cdot m^{-3}}$ $R_{\phi 1} = 0.0015\ \mathrm{m}$ $R_{\phi 2} = 0.0015\ \mathrm{m}$ $R_{\phi 3} = 0.0015\ \mathrm{m}$ $\frac{d\vec{\vec{\sigma}}}{dT} = -0.00005263\ \mathrm{N \cdot m^{-1} \cdot K^{-1}}$

https://doi.org/10.52202/069564-0033

Table 2. Material properties in the considered simulations.

Material	Density, ρ $(\mathrm{kg \cdot m^{-3}})$	Specific heat capacity, c_p $(\mathrm{J \cdot kg^{-1} \cdot K^{-1}})$	Thermal conductivity coefficient, k_{eff} $(\mathrm{W \cdot m^{-1} \cdot K^{-1}})$	Dynamic viscosity, μ $(\mathrm{Pa \cdot s})$	References
Borosilicate glass	2124.9	779.74	$0.9245251 + 0.0004777689 \cdot T + 9.178795 \cdot 10^{-7} \cdot T^2$	-	[22,23]
Gold nanorods	19320	129.81	317	-	[24,25]
Air	$352.965 \cdot T^{-1}$	1006.43	$0.004204762 + 7.242857 \cdot 10^{-5} \cdot T$	$7.29 \cdot 10^{-6} + 4.0 \cdot 10^{-8} \cdot T$	[26-28]
Glue	1231	1100	0.50	0.30	[29,30]

4. Results

Heat transfer results may be described by the mathematical functions whose solutions are determined by specified boundary conditions. Some results are based on Green's or gaussian functions and are presented in [19 – 20]. The presence of forced and natural convection, however, which occurs in this work, implies the major functions' complicity and therefore numerical methods are advisable.

Results are being considered 5 μm above (top) (red color) and under (bottom) (blue color) glassy base, near the AuNRs platforms respectively. Fig. 3a. highlights maximum temperature vs time response, fig. 3b. presents the entropy changes, whereas fig. 3c outlines maximum velocity fluctuations. As may be noticed, maximum temperature reaches 33.225°C and 31.795°C above and under the top glass respectively, which is a promising temperature increase since the operating laser power is quite low. It is expected that higher values of power would significantly increase the maximum temperature of the system. On the other hand, this work assumes using the three wavelengths which do not correspond perfectly for the sun spectrum distribution.

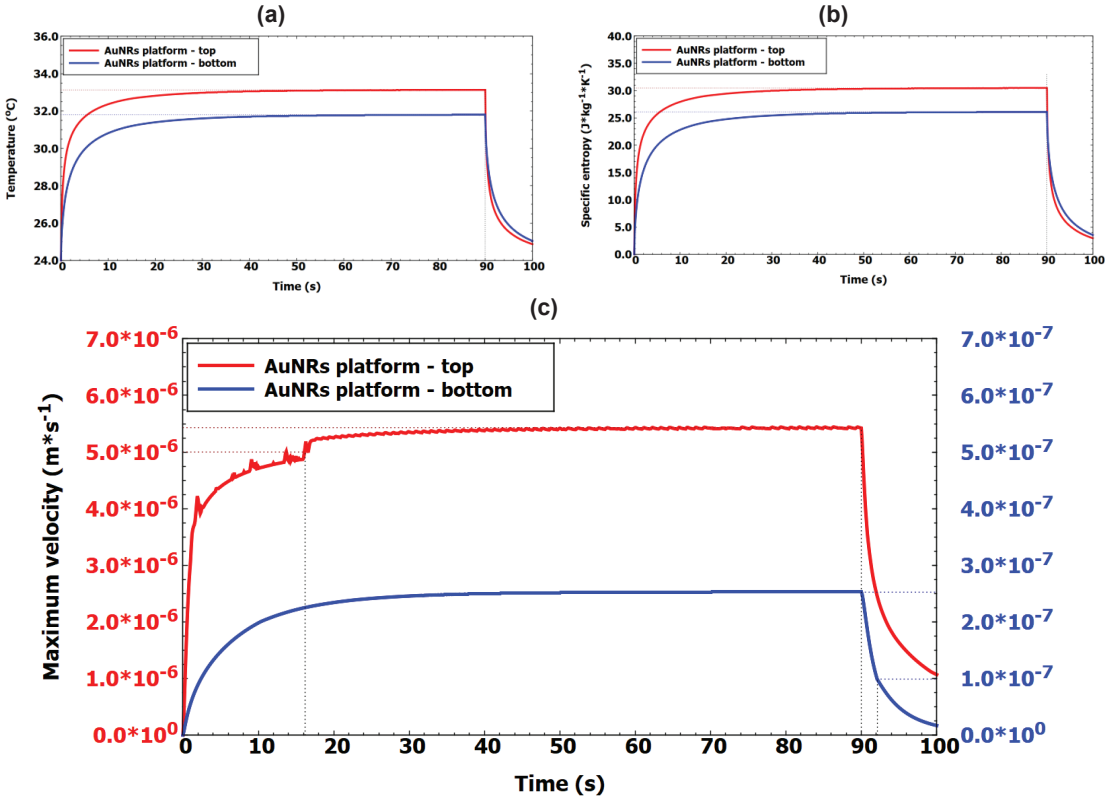

Figure. 3. (a) Maximum temperature, **(b)** specific total entropy and **(c)** maximum velocity vs. time results 5 μm above (top) (red color) and 5 μm under (bottom) (blue color) glassy base of the AuNRs platforms respectively. Using dotted lines, sensitive moments in time are raised.

https://doi.org/10.52202/069564-0033

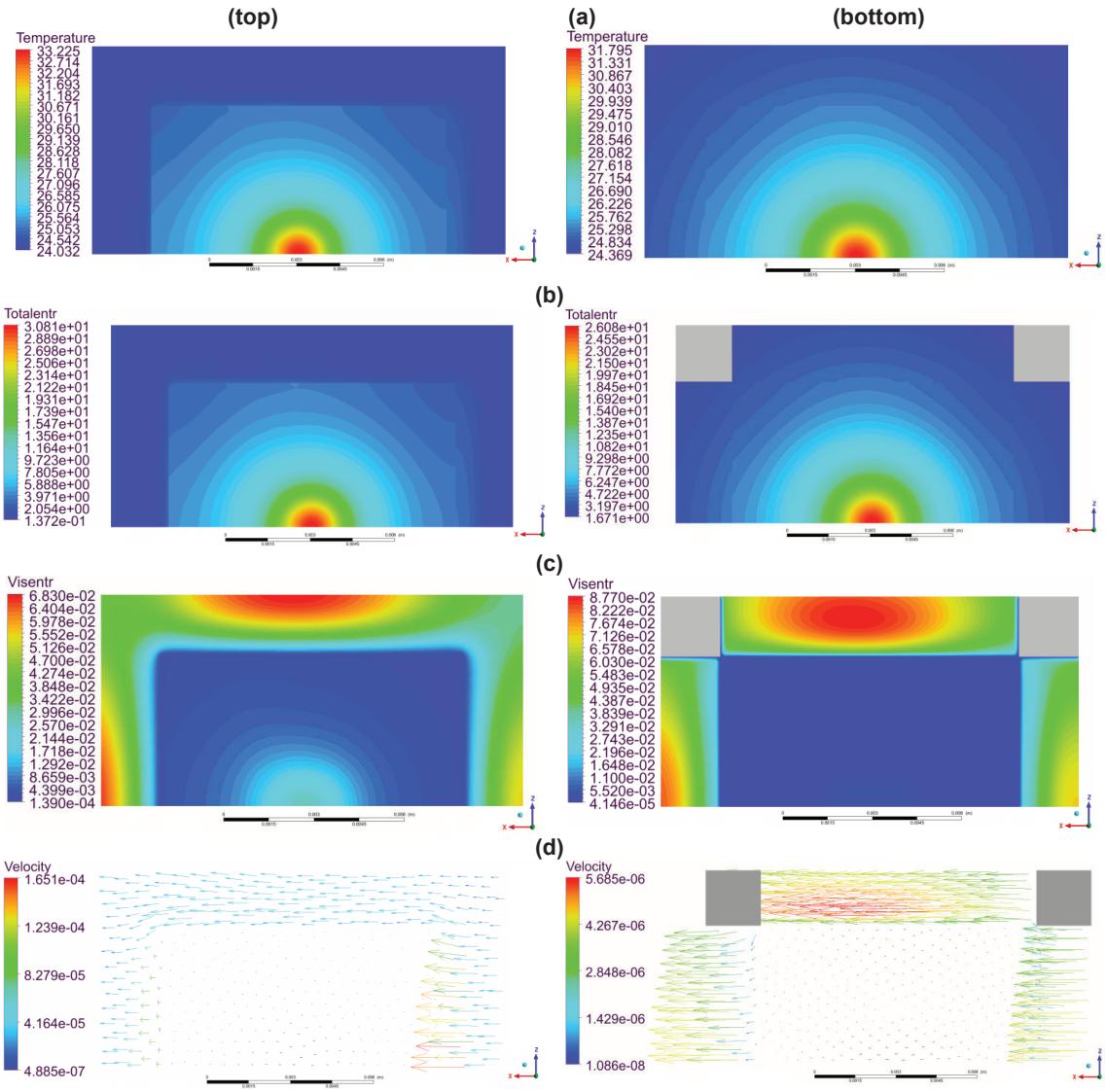

Figure. 4. (a) Temperature, **(b)** specific total and **(c)** dynamic entropy, **(d)** velocity contour plots 5 μm above (top) (red color) and 5 μm under (bottom) (blue color) glassy base of the AuNRs platforms respectively after 90 seconds of the system irradiation.

Furthermore, curve shapes are responsible for the heat rate and thermal properties of that the considered system consisted. As long as the quick temperature increase is explained via high value of material's thermal diffusivities compared to gold, the steady state is obtained as a result of assumed adiabatic and insulated conditions at walls and of the air domains, respectively. Nonetheless, under the discussed theory in Appendix A, many parameters, like nanoparticle's dimensions or surface material, can be adjusted ensuring different temperature changes and curve shapes. Each of these aspects should be examined particularly in the near future.

Likewise, the obtained low values of velocity imply weak impact on the heat rate. As a matter of fact, thermal effects may have triggered the natural convective movement of the fluid associated with the distribution of the plate. Moreover, the results are expected to be distinguishable in the microscale region between glass and above the AuNRs-platform respectively. This may be noticed peering into both the differences of the maximum temperature and specific entropy for the considered surfaces. The explanations are searched in the thickness of the AuNRs platforms and the heat transfer coefficient which implies a lower value if the flow is weaker, which is clearly visible in fig. 3c. The flow, however, is governed by different phenomena. The top-AuNRs-platform is exhibited for the forced convection and turbulence effects which is due to the gravity forces.

https://doi.org/10.52202/069564-0033

This is the reason why dynamic entropies, which are presented in figs. 4c and 5c, are distinguishable to each other, and why are visible only very close to AuNRs platforms. In order to enforce the flow inside the microscale region, significantly higher pressures should be applied, which is not necessary for the top-AuNRs-platform due to the assumed outlet condition. On the other hand, dynamic entropy is not a dominant process, which may be realized from total entropy contours which implies that and mainly heat transfer does the lion's share in the whole simulation.

Hence, heat is generally transported by conduction, whereas natural convection is directly responsible for the entropy generation. Dynamic entropy, which is caused by friction, is a few ranks lower than the static one. However, asymmetrical heat wave front, which is visible in the figures 4c and 5c, appears to be due to the natural convection, both near the top- and bottom-AuNRs-platforms.

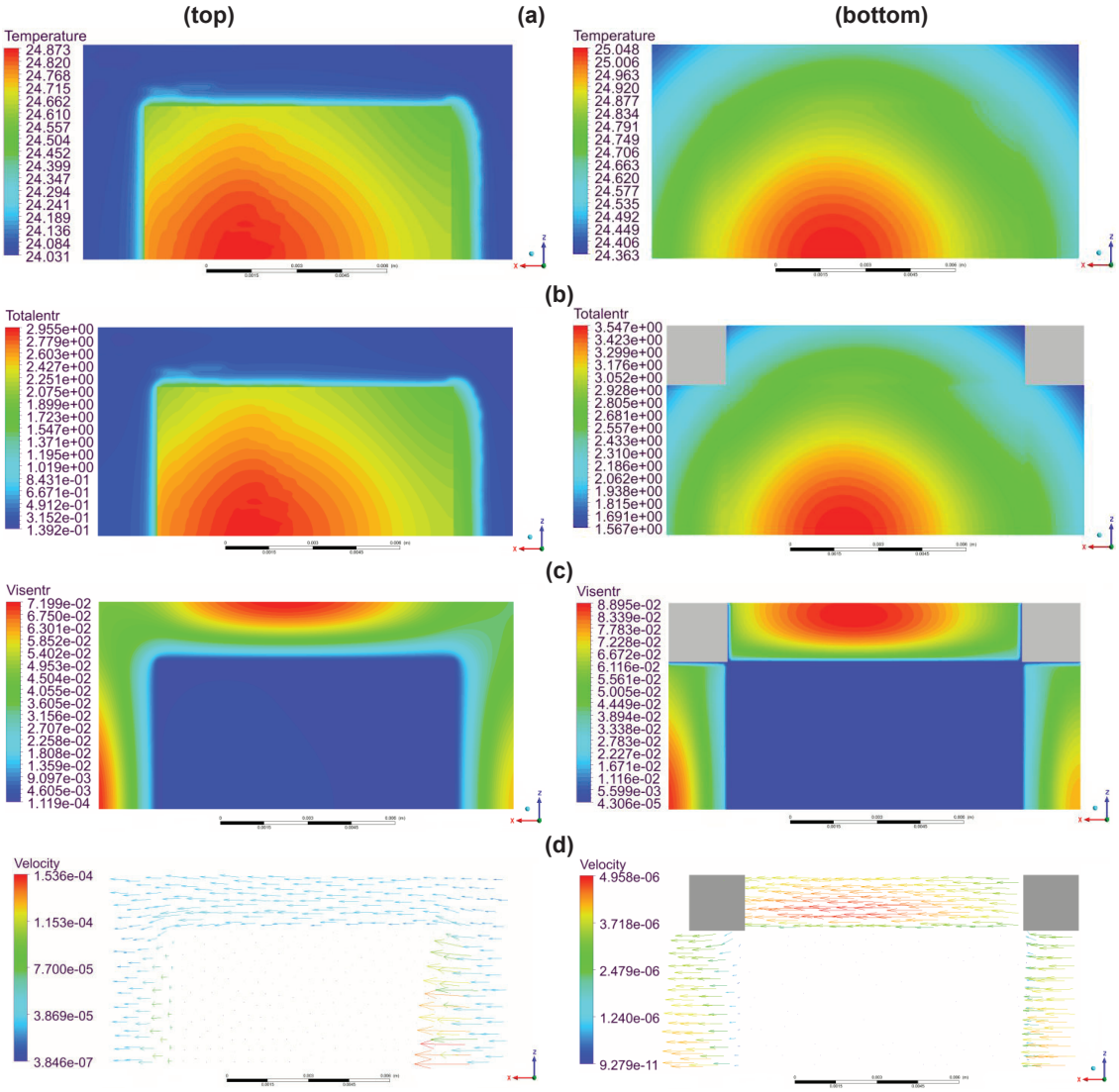

Figure. 5. (a) Temperature, **(b)** specific total and **(c)** dynamic entropy, **(d)** velocity contour plots 5 μm above (top) (red color) and 5 μm under (bottom) (blue color) glassy base of the AuNRs platforms respectively after 10 seconds of the system cooling.

Jagged contours may be explained following that Marangoni's stress is responsible for the fluctuations presence which are intensified as a result of the turbulence effects due to convection forces. Moreover, it is supposed that heat is transported as a result of the convection processes which implies the turbulence influence, even if the flow takes low values. Another issue occurs at the rectangular boundaries where the contours appear to be discontinuous due to the fact that there are located the material boundaries, and the material properties abruptly vary. These discontinuities are common phenomena manifested at the micro- and

nanoscale, with velocity slip, transpiration mobility and Marangoni's stress among the dominant effects [36-39].

Furthermore, the jumpy variations may be noticed in the velocity vs time plot where the curve does not possess a smooth character. This is not observed in the bottom-AuNRs platform where the curve is deprived of the discontinuities, and where the turbulence is significantly weaker. It is also worth mentioned that the curves have been improved via decreasing mesh size as long as the satisfactory quality obtains, and every simulation has provided a similar feedback.

5. Summary

Metallic nanostructures, although they are followed with standard Boltzmann transport equations, require utilizing sophisticated mathematics which implies the problem complexity in boundary conditions. In this work, microscale heat transfer and convection moves have been raised and discussed. This paper suggests that there is a possibility to apply metallic nanoparticles in real energy or biomedical applications. Their unquestionable advantage is heating them inside pipes, which omits the problem of the low heat transfer coefficient of the exterior surfaces. Moreover, the utilized model, although NRs are not truly present, the interaction between NRs and light is the response based on the physical phenomena. The approach, however, does not require to calculate many equations, which definitely may accelerate the simulation compared to the available full optical approaches, like DO model.

Furthermore, the outlined theoretical results reveal that even relatively low values of the laser powers are sufficient so as to obtain a significant temperature increase. In this work, the maximum value has reached ΔT=9.225^{o}C. Although higher temperature may be provided by manipulation of nanoparticle's properties or stronger light sources, it should be taken into account the heat transfer is strictly conjugated with the conduction where heat spreads decreasing the maximum value supporting the average one. On the other hand, the competition between force and natural convection also is not trivial, which has been present and been studied thoroughly in this work as well. In this work, the forced convection influence has been discovered not to do the lion's share due to the weak flow near the AuNRs platforms.

It is being predicted, however, this effect would be much more visible e.g. in solar collectors where AuNRs shall move freely and be exposed to the high stresses due to the forced convection. Nonetheless, the considered topic takes the advantage and encourages further investigations due its promising temperature increase in the imitating-systems which may be used in energy or biomedical applications.

Acknowledgments

The work was supported by the National Science Centre, Poland, under research project „Shape and displacement optimization of gold nanorods in the killing chamber in order to phototermoablation processes", no UMO-2021/43/D/ST8/02504.

Computations were carried out using the computers of Centre of Informatics Tricity Academic Supercomputer & Network (CI TASK) in Gdansk.

Appendix A

This part studies the applied formula for electrical polarizabilities applied for the substrate effect of the used nanostructures. Due to the surface effect and anisotropy of considered nanostructures, several formulas are calculated and specified for 130 x 130 different sizes of d_{s_i} and d_{l_i}. The general boundary condition for the total polarizability is described as follows:

$$\alpha_i = \frac{2}{3}\left(\frac{2}{3}\cdot\left(\left(\alpha_{i,y}\right)_{Ya}+\left(\alpha_{i,z}\right)_{Ya}\right)+\frac{1}{3}\cdot\left(\left(\alpha_{i,x,dl}\right)_{Ya}\right)\right)+\frac{1}{3}\cdot\left(\frac{2}{3}\cdot\left(\left(\alpha_{i,y,ds}\right)_{Ya}+\left(\alpha_{i,z,ds}\right)_{Ya}\right)+\frac{1}{3}\cdot\left(\left(\alpha_{i,x}\right)_{Ya}\right)\right) \quad \text{(A.1)}$$

The substrate and distance effects are described by Royer-Yamaguchi approach [15 -16], where the anisotropic factor, β_i, is perpendicular along the y-axis, as follows:

$$\left(\alpha_i\right)_{Yam} = \frac{\left(\alpha_i\right)_{sur}}{1+\left(\frac{\left(\alpha_i\right)_{sur}}{\frac{4}{3}\pi\cdot {d_{s_{1i}}}^2\cdot d_{l_{1i}}}\right)\cdot\beta_i} \quad \text{(A.2)}$$

Surface polarizabilities are assumed for the prolate ellipsoids which are the complex functions, as follows:

$$\left(\alpha_{i,x,z}\right)_{sur}\rightarrow\left(\alpha_{i,x,z}\right)_{sur}\left(\mathbb{p}_{11},\mathbb{q}_{11},\mathbb{e}_{11},\varepsilon_h,\varepsilon_{sur},d_{s_{1i}},d_{s_{2i}},d_{l_{1i}},u_l\right) \quad \text{(A.3)}$$

$$\left(\alpha_{i,y}\right)_{sur}\rightarrow\left(\alpha_{i,y}\right)_{sur}\left(\mathbb{p}_{10},\mathbb{e}_{10},\varepsilon_h,\varepsilon_{sur},d_{s_{1i}},d_{s_{2i}},d_{l_{1i}},u_l\right) \quad \text{(A.4)}$$

Contrary to ellipsoids, rods possess the flat long dimension which contributes to appear new dipole configurations. It was discovered by Fuchs publication [18] in which the charge arrangements of edgy shapes (triangles, cubes, octahedrons etc.) The publication implies that the dipole arrangement in a nanoparticle may be

https://doi.org/10.52202/069564-0033

specified by a certain parameter in order to solve and establish the other dipole configurations. As long as the along axes tend to spherical distribution, $(\phi_i(d_{s_i}, d_{l_i}) \rightarrow \phi_i(d_{s_i}, d_{s_i}) \rightarrow 0)$, the situation changes in rods. It is assumed to exist the new configuration where dipoles are arranged at the very opposites diagonal indicating $\phi_i(d_{s_i}, d_{l_i}) \rightarrow \phi_{i,d_l}\left(d_{l_i} - d_{s_i}, \sqrt{(d_{l_i} - d_{s_i})^2 + (d_{s_i})^2}\right)$ and $\phi_i(d_{s_i}, d_{l_i}) \rightarrow \phi_{i,d_s}\left(d_{s_i}, \sqrt{(d_{l_i} - d_{s_i})^2 + (d_{s_i})^2}\right)$, which are projected on the main space diagonal of a rod for y- and x-, z- axes respectively. Fig. A.1 demonstrates these four assumed charge arrangements which have been adjusted to the x-oriented particles than are deposited on the y-axis surface. The assumed parameters and properties for the abovementioned formulas are highlighted in tables A.1 and A.2.

Table A.1: Nanorods assumed parameters

General parameters	**Assumed value**
NPs general size, d_s x d_s x d_l	15 x 15 x 55 nm
Coating thickness, d_{s_2}	4 nm
Average NP – NP distance, u_l	140 nm
Nanoparticles concentration, ξ	$8.67 \cdot 10^{21}$ m^{-3}

Table A.2: Electrical properties for the utilized three wavelength values

Wavelength dependence parameters		$\lambda_1 = 532$ nm	$\lambda_2 = 640$ nm	$\lambda_3 = 808$ nm	**References**
Permittivity of air (humidity – 15%), ε_h		1.103112	1.102395	1.101639	[30,32]
Permittivity of borosilicate glass, ε_{sur}		2.308880	2.294619	2.281912	[22]
Gold electrical permittivity, ε_1	$\mathbb{re}$	-4.660220	-12.183069	-25.035329	[31]
	$\mathbb{im}$	2.346720	1.1734087	1.564609	

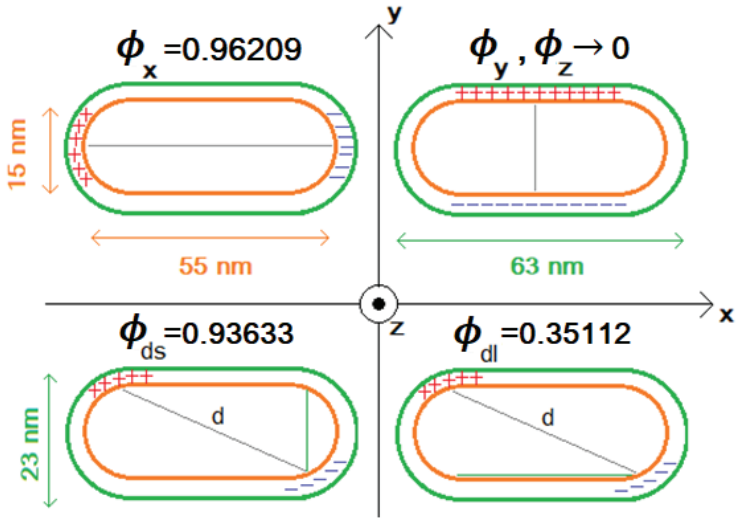

Figure. A.1. Electric dipole configurations which have been considered in the calculations for 15-15-55-nm gold nanorods (orange color) coated by a 4-nm organic compound (green color).

Nomenclature

Roman letters

A_{abs_i}	absorption coefficient of the i-particle, m^{-1}
A_{abs_M}	absorption coefficient of the continuous material, m^{-1}
C_{abs_i}	absorption cross section of the i-particle, m^2
C_{ext_i}	extinction cross section of the i-particle, m^2
C_{sca_i}	scattered cross section of the i-particle, m^2
c_p	specific heat capacity, $\mathrm{J} \cdot \mathrm{K}^{-1} \cdot \mathrm{kg}^{-1}$
$\vec{d}$	symmetric rate of deformation, s^{-1}
d_{l1_i}	longer diameter of the i-nanoparticle, m

https://doi.org/10.52202/069564-0033

d_{s1_i}	shorter diameter of the i-nanoparticle, m
d_{s2_i}	size of the nanoparticle's coating, m
e	specific energy, $\mathrm{J} \cdot \mathrm{kg}^{-1}$
$G_{\mathbb{k}}$	turbulence kinetic energy generation due to velocity gradients, $\mathrm{kg} \cdot \mathrm{m}^{-1} \cdot \mathrm{s}^{-3}$
$G_{\text{Б}}$	turbulence kinetic energy generation due to buoyancy forces, $\mathrm{kg} \cdot \mathrm{m}^{-1} \cdot \mathrm{s}^{-3}$
$\vec{g}$	gravity, $\mathrm{m} \cdot \mathrm{s}^{-2}$
h	heat transfer coefficient, $\mathrm{W} \cdot \mathrm{m}^{-2} \cdot \mathrm{K}^{-1}$
$I_o(\vec{r})$	initial intensity laser profile, $\mathrm{W} \cdot \mathrm{m}^{-2}$
I_{abs_i}	absorbed part of the i-particle, $\mathrm{W} \cdot \mathrm{m}^{-2}$
$I_{\vec{d}}$	first invariant of the strain rate, s^{-1}
$\overleftrightarrow{I}$	unit tensor, -
k_{eff}	effective thermal conductivity coefficient, $\mathrm{W} \cdot \mathrm{m}^{-1} \cdot \mathrm{K}^{-1}$
L	subsequent laser source
l_{ph}	light-NR interaction thickness, m
$Pr_{\mathbb{k}}$	turbulent Prandtl number for kinetic energy, -
Pr_{ϵ}	turbulent Prandtl number for rate of dissipation, -
Pr	Prandtl number, -
p	pressure (Pa)
R_i	reflection coefficient of the i-nanoparticle, m
R_M	reflection coefficient of the continuous material, m
$R_{\phi L}$	beam sizes of laser sources, m
$\overleftrightarrow{R}$	Reynolds stress tensor
$\vec{r}$	radius – spherical coordinate, m
S_e^f	source of energy for fluids, $\mathrm{W} \cdot \mathrm{m}^{-3}$
S_e^{np}	source of energy for the i-particle, $\mathrm{W} \cdot \mathrm{m}^{-3}$
T	temperature, K
T_o	initial temperature at the $t = 0\ \mathrm{s}$, K
t	time, s
u_l	distance between particles, m
$\vec{v}$	velocity of the fluid, $\mathrm{m} \cdot \mathrm{s}^{-1}$
v_{sound}	speed of sound, $\mathrm{m} \cdot \mathrm{s}^{-1}$
$\overrightarrow{X^{\dagger}}$	diffusive momentum flux, $\mathrm{kg} \cdot \mathrm{m} \cdot \mathrm{s}^{-2}$
x, y, z	Cartesian's coordinates, -

Greek letters

α_i	polarizability of the i-particle, m^3
β	anisotropic factor for distance and surface effects, -
δ	thickness of the considered material, m
ε_h	permittivity of the host medium, -
ε_{sur}	permittivity of the base where NRs are embedded, -
ϵ	turbulent energy dissipation, $\mathrm{m}^2 \cdot \mathrm{s}^{-3}$
λ	incident wavelength, m
μ	molecular viscosity, $\mathrm{Pa} \cdot \mathrm{s}$
μ_{t}	eddy viscosity, $\mathrm{kg} \cdot \mathrm{m}^{-1} \cdot \mathrm{s}^{-1}$
ξ	nanoparticles concentration, m^{-3}
ρ	density of a material, $\mathrm{kg} \cdot \mathrm{m}^{-3}$
$\vec{\sigma}$	surface tension parameter, $\mathrm{N} \cdot \mathrm{m}^{-1}$
ψ	prolation parameter, -

Slavic letters

Б	thermal expansion coefficient, K^{-1}
г	relaxation time, s

Others

∂	symbol of partial derivative
$\mathbb{i}$	symbol of imaginary unit
$\mathbb{im}$	imaginary part of a complex expression
$\mathbb{k}$	turbulent kinetic energy
$\mathbb{p}$	associated Legendre polynomials of a first kind
$\mathbb{q}$	associated Legendre polynomials of a second kind
$\mathbb{re}$	real part of a complex expression

https://doi.org/10.52202/069564-0033

Subscripts and superscripts

a	air
d	diffusivity
f	fluid
i	selected number
l	long or distance
M	material
o	in reference to initial conditions
s	short
t	turbulent
†	transposition

Abbreviations

abs	absorption
div	divergence
eff	effective
exp	exponent
ext	extinction
grad	gradient
np	nanoparticle
NRs	nanorods
ph	photon
sca	scattering
sur	surface
Ya	in reference to Yamaguchi approach

References

[1] Coyle E. D., Simmons R.A, Understanding the Global Energy Crisis, Purdue University Press, West Lafayette, USA, 2014

[2] Petronella F., De Biase D., Zaccagnini F., Verrina V., Lim S., Jeong K., Miglietta S., Petrozza V., Scognamiglio V., Godman N.P., Evans D.R., McConneye M., De Sio L., Label-free and reusable antibody-functionalized gold nanorod arrays for the rapid detection of Escherichia coli cells in a water dispersion, Environmental Science: Nano, 2022, 9, 3343-3360

[3] Pontico M.,Conte M., Petronella F., Frantellizzi V., De Feo M.S., Di Luzio D., Pani R., De Vincentis G., De Sio L., 18F-fluorodeoxyglucose (18F-FDG) Functionalized Gold Nanoparticles (GNPs) for Plasmonic Photothermal Ablation of Cancer: A Review, Pharmaceutics, 2023, 15, 319

[4] Mikielewicz D., Hydrodynamics and heat transfer in bubbly flow in the turbulent boundary layer, International.Journal of Heat and Mass Transfer, 2002, 46, 207 – 220, 2

[5] Ziolkowski P., Badur J., A theoretical, numerical and experimental verification of the Reynolds thermal transpiration law, International Journal of Numerical Methods for Heat & Fluid Flow, 2018, 28, 1

[6] De Sio L., Placido T., Comparelli R., Curri M. L., Striccoli M., Tabiryan N., Bunning T. J., Next-generation thermo-plasmonic technologies and plasmonic nanoparticles in optoelectronics, Progress in Quantum Electronics, 2015, 41, 23

[7] Sobhan C.B, Peterson G.P., Microscale and Nanoscale Heat Transfer: Fundamentals and Engineering Applications, CRC Press Taylor&Francis Group, USA, 2008

[8] Cattaneo M.C., A form of heat conduction equation which eliminates the paradox of instantaneous propagation, Compte Rendus, 1958, 247, 431–433

[9] Bohren C.F., Huffman D.R., Absorption and Scattering of Light by Small Particles, A Wiley-Interscience publication, Canada, 1998

[10] Strutt, J.W. (Rayleigh L.), On the scattering of light by small particles, The London, Edinburgh, and Dublin Philosophical Magazine and Journal of Science, 1871, 41, 275, 447 – 454

[11] Radomski P., Ziolkowski P., Mikielewicz D., Theoretical approach of laser-irradiated metallic nanoparticles in selected mixed-convection systems, Progress in heat and mass transfer research, Conference monograph of XVI Heat and Mass Transfer Symposium in Mragowo, Polish Academy of Science (PAN), Bialystok, 2022, 374 – 384

[12] Radomski P. Ziolkowski P., De Sio L., Mikielewicz D., Effects of the laser-ablated metallic nanoparticles shapes on the photo-thermal performances in a selected fluidic medium, 15th Mediterranean Workshop and Topical Meeting "Novel Optical Materials and Applications", University of Calabria, Cetraro (Italy), 2022

[13] Smoluchowski M., On conduction of heat by rarefied gases, Annalen der Physik, 1898, 300, 1
[14] Radomski P., Ziolkowski P., De Sio L., Mikielewicz D., Computational fluid dynamics simulation of heat transfer from densely packed gold nanoparticles to isotropic media, Archives of Thermodynamics, 2021, 42, 87 – 114, 3
[15] Yamaguchi T., Yoshida S., Kinbara A.,Optical Effect Of The Substrate On The Anomalous Absorption Of Aggregated Silver Films, Thin Solid Films, 1974, 21, 173 – 187
[16] Royer P., Bijeon J.L., Goudonnet J.P., Inagaki T., Arakawa E.T., Optical Absorbance of Silver Oblate Particles, Substrate And Shape Effects: Surface Science, 1989, 217, 384 – 402
[17] Roache, P.J., Quantification of Uncertainty in Computational Fluid Dynamics, Annual Review of Fluid Mechanics, 1997, 29, 123 – 160
[18] Fuchs R., Theory of the optical properties of ionic crystal cubes, Physical Review B, 1975, 11, 1732 – 1740, 4
[19] Domański R., Laser Radiation – solid-state interaction, Polish Scientific-Technical Journals, 1990, Warsaw (Poland), 130 – 220 (in Polish)
[20] Carslaw H.S, Jaeger J.C, Conduction of Heat in Solids. Second Edition, Oxford University Press, 1959, London, 50–132
[21] Romanchuk B.J., Computational Modeling of Buble Growth Dynamics in Nucleate Pool Boiling for Pure Water and Aqueous Surfactant Solutions, Master of Engineering dissertation, Division of Research and Advanced of The University of Cincinnati, 2014
[22] Bansal N. P., Doremus R. H., Handbook of Glass Properties, Academic Press, Materials Engineering Department Rensselaer Polytechnic Institute, Troy, New York, 1986
[23] Zaitlin M. P., Anderson A. C., Thermal Conductivity of Borosilicate Glass, Physical Review Letters, 1974, 33, 1158-1161, 19
[24] Reddy H., Temperature-dependent optical properties of gold thin films, Optical Material Express, 2016, 6, 2776 – 2802, 9
[25] Siegel R., Howell J.R., Thermal radiation heat transfer, McGraw-Hill Book Company, USA, 1972
[26] Engineering ToolBox, (2003). Air - Density, Specific Weight and Thermal Expansion Coefficient vs. Temperature and Pressure [accessed 17.2.2023].
[27] Engineering ToolBox, (2009). Air - Thermal Conductivity vs. Temperature and Pressure [accessed 17.2.2023].
[28] Engineering ToolBox, (2003). Air - Dynamic and Kinematic Viscosity [accessed 17.2.2023].
[29] Mark J. E., Polymer Data Handbook, Oxford University Press, 1999, 131, 44
[30] Bengte D. L., The Refractive Index of Air, Metrologia,1966, 8, 71 – 80, 2
[31] Vial A., Laroche T., Description of dispersion properties of metals by means of the critical points model and application to the study of resonant structures using the FDTD method, J. Phys. D: Appl. Phys, 2007, 40, 7152–7158
[32] Fernández-Prini R., Release on the Refractive Index of Ordinary Water Substance as a Function of Wavelength, Temperature and Pressure, The International Association for the Properties of Water and Steam, Erlagen, 1997, 2 – 7
[33] Bejan A., Fundamentals of Exergy Analysis, Entropy Generation Minimization, and the Generation of Flow Architecture, International Journal of Energy Research, 2002, 26, 1–43.
[34] Sciubba E., Use of Exergy Analysis To Compute The Resource Intensity of Biological Systems and Human Societies, 12th Joint European Thermodynamics Conference, Brescia, 2013, 268 – 273
[35] Jou D. Entropy, entropy flux, temperature, and second law in extended irreversible thermodynamics, 12th Joint European Thermodynamics Conference, Brescia, 2013, 211 – 216.
[36] Ziolkowski P., Badur J., On Navier slip and Reynolds transpiration numbers, Archive of Mechanics, 70, 3, 2018, 269–300.
[37] Schneider W., Surfaces as non-autonomous thermodynamic systems, 12th Joint European Thermodynamics Conference, Brescia, 2013, 178 – 185.
[38] A. Sellitto, V. A. Cimmelli and D. Jou, Thermoelectric effects and size dependency of the figure-of-merit in cylindrical nanowires, Int. J. Heat Mass Transfer, 57, 2013, 109-116.
[39] D. Jou, J. Casas-Vazquez and G. Lebon, Extended Irreversible Thermodynamics, Berlin Springer, fourth revised ed., 2010

https://doi.org/10.52202/069564-0033